51st AIAA Aerospace Sciences Meeting including the New Horizons Forum and Aerospace Exposition
07 - 10 January 2013, Grapevine (Dallas/Ft. Worth Region), Texas

AIAA 2013-0688

Development of Discontinuous Galerkin Method for Detonation and Supersonic Combustion

Yu Lv[*] and Matthias Ihme[†]

Department of Aerospace Engineering, University of Michigan, Ann Arbor, MI 48109, USA

A discontinuous Galerkin algorithm for the simulation of realistic detonation and super-sonic combustion systems is developed. This algorithm enables to consider complex and temperature/mixture-dependent thermodynamic transport properties, detailed and stiff reaction chemistry, and the robust shock-capturing. In order to evaluate all relevant algorithmic aspects, the DG-method is applied to a series of test-cases of increasing physical complexity: Begin with binary thermal advection and multi-species shock-tube problems, the accuracy and conservation properties of the double-flux formulation and the shock-capturing scheme are investigated. Following this analysis, simulations of a multi-species Argon-diluted Hydrogen/Oxygen detonation system are conducted using a detailed chem-ical kinetics mechanism. By considering refinement in polynomial order, mesh-refinement, and comparisons with second-order FV-solution, it is shown that optimal convergence rates are achieve and that polynomial refinement provides advantages in better resolving the Zeldovich-Neumann-Döring (ZND) flame structure behind the shock.

I.   Introduction

Motivated by the interest in the fundamental analysis, the utilization, and the control of detonation and high-speed combustion, significant progress has been made in developing modeling techniques and algo-rithms for predicting supersonic combustion. However, the accurate prediction of these combustion-regimes introduces the following challenges. First, detonation waves are inherently combustion-driven shock-waves, requiring adequate and stable numerical schemes for capturing shock-discontinuities. On the other side, higher-order schemes are beneficial in smooth regions away from shocks. Second, combustion-processes in general requires the consideration of a large number of scales which can differ by several orders. Examples for this are highly reactive radical species, pollutant-concentrations in the parts-per-million range, or major product species, such as water or carbon dioxide, that are formed on chemically slow times scales in the post-reaction zone. This disparity in chemical time-scales introduces numerical stiffness, which requires the consideration of efficient temporal integration schemes. The fourth issue of consideration is that the reaction zone is confined to a narrow region on sub-millimeter scales. Since this reaction zone controls the flame-propagation, combustion-dynamics, heat-release, and fuel-conversion, it is necessary to accurately resolve this region. Finally, combustion requires the consideration of thermodynamic properties that depend on the local species composition and temperature. This is illustrated in Fig. 1, showing the ratio of specific heats as function of temperature for difference chemical species. Consideration of these temperature-dependent mixture properties is critical for the prediction of the flame-temperature and location of the reaction zone. However, the consideration of nonuniform thermal properties in numerical flux-based formulations introduces significant challenges, and – if inconsistently treated – result in numerical oscillations and loss of conservation properties of the numerical schemes.

The objective of this contribution is to develop a numerical algorithm that addresses these challenges. To this end, a discontinuous Galerkin (DG) formulation is considered. Compared to lower-order finite-difference (FD)/finite-volume schemes (FV), DG-methods offer several advantages: In particular, the DG method (i) allows for arbitrarily high order of accuracy that is determined through the selection of the basis functions; (ii) is able to capture discontinuities and strong gradients of the solution; (iii) enables a compact

---

[*]Research Assistant, Department of Aerospace Engineering, University of Michigan, and AIAA Member.
[†]Assistant Professor, Department of Aerospace Engineering, University of Michigan, and AIAA Member
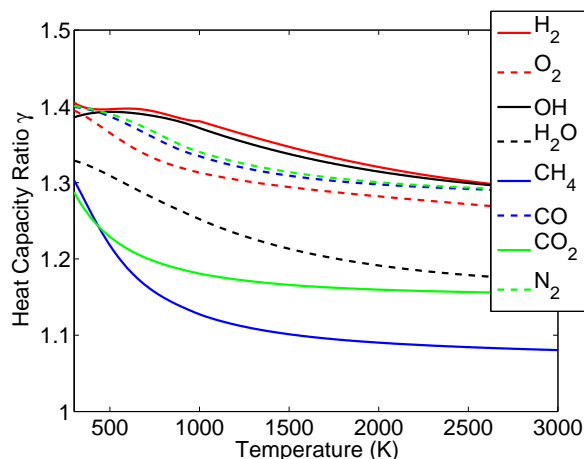
American Institute of Aeronautics and Astronautics

Figure 1. Ratio of specific heats as function of temperature for different chemical species.

discretization that is, unlike to conventional FD and FV methods, confined to the local element; (iv) is well suited for advanced refinement strategies utilizing both local mesh-adaption and refinement in polynomial order (hp-refinement); and (v) exhibits optimal convergence properties.

In the following, a DG-algorithm for simulating chemical-reacting flows is developed. Special focus is hereby attributed to applications to realistic detonation and supersonic combustion problems under consideration of complex reaction chemistry and detailed transport. The evolution of these combustion systems is described by the reacting Euler equations. The key ingredients of the developed DG-algorithm are the utilization of a double-flux function for the description of multicomponent flows,[1] a splitting scheme for treating stiff chemical reaction, a shock-capturing scheme,[2] and the evaluation of thermo-viscous-diffusive transport properties and reaction rates using detailed chemical-kinetics libraries.[3]

The remainder of this paper has the following structure. The governing equations are presented in Sec. II and algorithmic developments regarding the treatment of non-uniform transport properties, time-integration, and shock-capturing scheme are discussed in Sec. III. The reacting DG-scheme is subsequently applied to a series of test-configurations of increasing physical complexity to demonstrate the accuracy and capability of this algorithm. The paper finishes with conclusions and a discussion of further research directions.

II.   Governing Equations

The reactive Euler equations for multi-species combustion can be written in the following form:

$$\partial_t(\rho Y_i) + \partial_j(\rho Y_i u_j) = \dot{\omega}_i, \tag{1a}$$

$$\partial_t(\rho u_i) + \partial_j(\rho u_i u_j) + \partial_i p = 0, \tag{1b}$$

$$\partial_t(\rho E) + \partial_j[(\rho E + p)u_j] = 0, \tag{1c}$$

where ρ, u_i, Y_j, E and p refers to the density, velocity of the ith component, mass fraction of species j, specific total energy, and pressure. The density is computed from the conservation of elemental density,

$$\rho = \sum_{j}^{N}(\rho Y_j), \tag{2}$$

and the specific total energy is defined as

$$E = \sum_{i=1}^{N} Y_i \left[h_{f,i}^0 + \int_{T_0}^{T} c_{p,i}(T)dT \right] + \frac{u_j^2}{2} - \frac{p}{\rho}, \tag{3}$$

in which T is the temperature and $h_{f,j}^0$ is the heat of formation of the jth species defined at reference temperature T_0; $c_{p,j}$ is the specific heat capacity at constant pressure of the jth species, which is a function

American Institute of Aeronautics and Astronautics

of temperature and evaluated through NASA polynomials. Eq. (1) is supplemented by the ideal gas law, relating pressure to density, temperature and species conservation.

$$p = \rho R_u T \sum_{i=1}^{N} \frac{Y_i}{M_i}, \tag{4}$$

where R_u is the universal gas constant, and M_i is the molecular weight of the ith species.

III.   Numerical Method

A.   Discontinuous Galerkin Discretization

The reactive Euler equation can be rewritten in index notation as:

$$\partial_t U_j + \partial_k F_{kj}^c - S_j = 0 \tag{5}$$

where U_j refers to the jth component of the conservative state vector, and F_{kj}^c is the inviscid flux for the jth component of the state vector in the kth spatial direction; F_{kj}^c is a non-linear function of the full state vector.

Eq. (5) is locally discretized in a discontinuous Galerkin (DG) spaces. For this, the computational domain Ω is subdivided into a set of elements $\{e\}$ and the solution of the reactive Euler equations is restricted to be represented by polynomial. We then approximate each component of the conservative vector by the following space,

$$\Psi^h = \{\phi^h \in L_2(\Omega) \mid \phi^h|_{\Omega_e} \in \mathcal{P}_N(\Omega_e)\} \tag{6}$$

where $\mathcal{P}_N(\Omega_e)$ is a finite dimensional space on element non-overlapping Ω_e, here specified by set of polynomials with the order not larger than N. For the sake of clarity, we denote the spatial basis by ϕ, or its index form $\phi_{\{q\}}$, where the subscript q in braces refers to the qth component of the basis. Each component of the solution of Eq. (5), $\mathbf{U}$, can be approximated as

$$U_j(t, \mathbf{x}) = \sum_{q=1}^{N} \tilde{U}_{j\{q\}} \phi_{\{q\}}(\mathbf{x}), \tag{7}$$

where $\tilde{U}_{j\{q\}}$ refers to the component of the qth basis function. With this derivation, the problem reduces to solving for $\tilde{U}_{j\{q\}}$. To do that, Eq. (5) is multiplied by a test basis function $\phi_{\{q\}}$, followed by integral by parts. Finally we end up with the weak form:

$$\partial_t \tilde{U}_{j\{q\}} \int_{\Omega_e} \phi_{\{q\}} \phi_{\{q\}} d\Omega_e + \int_{\Omega_e} \phi_{\{q\}} \partial_k F_{kj}^c d\Omega_e - \int_{\Omega_e} \phi_{\{q\}} S_j d\Omega_e = 0 \tag{8}$$

where $\int_{\Omega_e} \phi_{\{q\}} \phi_{\{q\}} d\Omega_e$ is the mass matrix. The reaction term is local, and convection is treated using integration by parts,

$$\int_{\Omega_e} \phi_{\{q\}} \partial_k F_{kj}^c d\Omega_e = - \int_{\Omega_e} \partial_k \phi_{\{q\}} F_{kj}^c d\Omega_e + \int_{\partial\Omega_e} \phi_{\{q\}}^+ \hat{F}_{kj}^c (U_j^+, U_j^-) \hat{n}_k dS_e \tag{9}$$

where $\hat{n}_k$ is the outward pointing normal and $\partial\Omega_e$ represents the boundary of element Ω_e. On $\partial\Omega_e$, the notation $(^+)$ and $()^-$ refers to the quantities taken from the interior and exterior of element Ω_e, respectively. Elements in each direction are coupled through the flux function $\hat{F}_{kj}^c$. Here The convection flux is evaluated using a HLLC Riemann solver.[4]

B.   Algorithm for Non-uniform Thermal Properties

In chemically reacting flows, the dependence of the thermodynamic properties on temperature and composition cannot be neglected and requires accurate treatment. However, this issue is non-trivial,[5,6,7,8,9,10] and an inappropriate treatment may lead to spurious oscillations, which is a common issue when solving multi-fluid problem based on Godunov-type schemes. In the Discontinuous Galerkin framework, this issue

American Institute of Aeronautics and Astronautics

appears to be more severe, since spurious oscillations may have higher frequency content and amplitude with high-order spatial representation. An approach for handling this issue is the double flux model developed by Billet and Ryan.[1] In this model, the ratio of specific heat capacity γ is assumed to be constant in each finite element during each time step. The detailed algorithm consists of two steps, namely a energy projection and thermal property correction step.

In energy projection step, the specific heat is approximated using a piecewise linear function of temperature so that the energy term can be written in the form similar to a calorically perfect gas representation. We denote $c_p^m = a^m T + b^m, T \in [T^m, T^{m+1}]$, and the interval size determines the error which can be adjusted to reduce the error. With this extension, the enthalpy of each species can then be expressed as follows. For clarity, we drop the subscript here.

$$
\begin{aligned}
h^m &= h_0 + \sum_{k=0}^{m-1} \int_{T^k}^{T^{k+1}} (a^k T + b^k) dT + \int_{T_m}^{T} (a^m T + b^m) dT \\
&= h_0^m + \frac{a^m}{2}(T^2 - T^{m2}) + b^m(T - T^m) \\
&= h_0^m + a^m \frac{T^m + T}{2}(T - T^m) + b^m(T - T^m) \\
&\approx h_0^m + T \cdot (a^m T + b^m) - T^m(a^m T^m + b^m) \\
&= h_0^m - c_p(T^m)T^m + c_p(T)T \\
&= \widehat{h_0^m} + c_p(T)T
\end{aligned}
\tag{10}
$$

Where $\widehat{h_0^m}$ combines the heat of formation and the specific enthalpy from T_0 to T^m. With this simplification, the enthalpy formula becomes consistent to that of a calorically perfect gas. Finally, the specific total energy for the mixture can be written as:

$$
\begin{aligned}
E &= H - \frac{p}{\rho} \\
&= \sum_{i=1}^{N} \widehat{h_{0,i}^m} Y_i + \sum_{i=1}^{N} c_{p,i}(T)Y_i T + \frac{u_j^2}{2} - \frac{p}{\rho} \\
&= \sum_{i=1}^{N} \widehat{h_{0,i}^m} Y_i + \frac{p}{\rho(\gamma - 1)} + \frac{u_j^2}{2} \\
&= \widehat{h_0} + \frac{p}{\rho(\gamma - 1)} + \frac{u_j^2}{2}
\end{aligned}
\tag{11}
$$

where i indexes on species and j indexes on velocity components.

The second step involves the time integration, in which γ and $\rho\widehat{h_0}$ are frozen in each element during each individual step. With this, the gas mixture in each element is treated as a single-component calorically perfect gas. The flux at each element face is calculated twice, individually for left and right. After the velocity and pressure evolve without generating unphysical oscillations, all thermal properties are then updated using computed species mass fractions and temperature.

$$
\begin{aligned}
\mathbf{F}^+ &= F(\mathbf{U}^+, \mathbf{U}^-, \gamma^+, \rho\hat{h}_0^+), \tag{12a} \\
\mathbf{F}^- &= F(\mathbf{U}^+, \mathbf{U}^-, \gamma^-, \rho\hat{h}_0^-). \tag{12b}
\end{aligned}
$$

If $\gamma^+ \neq \gamma^-$, the flux is not fully conservative, but this conservation loss only affects the energy without influencing density and velocity. In Section IV, we will analyze this conservation loss, and it will be shown that this error remains small even for strong shock configurations. The quasi-conservative energy is marked as ρE^*. All variables, including ρE^*, can then be updated using any stable explicit time integration scheme combined with the above flux evaluation algorithm. At the end, pressure and kinetic energy are obtained from Eq. (11):

$$
p^{n+1} = (\gamma^n - 1)\left[(\rho E^*)^{n+1} - \frac{1}{2}(\rho u_j^2)^{n+1} - (\rho\hat{h}_0)^n\right],
\tag{13}
$$

American Institute of Aeronautics and Astronautics

Following this step, the heat capacity and enthalpy are updated, and finally the relaxed total energy is evaluated as:

$$Y_i^{n+1} = \frac{(\rho Y_i)^{n+1}}{\rho^{n+1}}, \tag{14a}$$

$$T^{n+1} = \frac{p^{n+1}}{R_u \sum \frac{\rho Y_i^{n+1}}{M_i}}, \tag{14b}$$

$$\gamma^{n+1} = \gamma(Y_i^{n+1}, T^{n+1}), \tag{14c}$$

$$\hat{h}_0^{n+1} = \hat{h}_0(Y_i^{n+1}, T^{n+1}), \tag{14d}$$

$$(\rho E^*)^{n+1} = \frac{p^{n+1}}{\gamma^{n+1}-1} + \rho^{n+1}\hat{h}_0^{n+1} + \frac{1}{2}(\rho u_j^2)^{n+1}, \tag{14e}$$

C. Treatment of Stiff Reaction Chemistry

The development of computationally efficient numerical schemes for combustion requires the consideration of the disparity of chemical species that evolve on vastly different time-scales. Therefore, a splitting scheme is used in which the non-stiff convection operator is advanced using an explicit scheme and the stiff chemical source terms are handled implicitly. The splitting scheme can formally be written as:

$$\mathbf{U}(t + \Delta t) = e^{0.5\Delta t F_k^c} e^{\Delta t S} e^{0.5\Delta t F_k^c} \mathbf{U}(t) \tag{15}$$

where the solution operator $e^{tF}u_0$ denotes $d_t u = F(u)$ with initial condition $u(0) = u_0$. In this scheme, the time step is solely controlled by the convection operator based on the CFL criterion. An ODE solver is employed in the reaction operator $e^{\Delta t S}$, and a strong-stability-preserving Runge-Kutta method[11] is used for advancing the convection operator $e^{\Delta t F_k^c}$.

D. Shock-Capturing Scheme

To represent discontinuities, a weighted essentially non-oscillatory (WENO) based limiter is used,[2] which shows good accuracy preserving property in smooth region and robust shock-capturing capabilities. This limiter first goes to detect the troubled elements, in which an adjustable constant M is introduced (The smaller M value is, the stricter the limiter is.).The, the limiter uses WENO idea to reconstruction a new solution polynomial for each individual troubled element based on the information from its corresponding neighbors. For example, if the element e_j requires limiting, the limited polynomial solution is obtained in the following way. Denote the DG solution polynomials of u on the cells e_{j-1}, e_j, e_{j+1} as $\mathcal{P}_{j-1}, \mathcal{P}_j, \mathcal{P}_{j+1}$, respectively. In order for the limited polynomial to hold the original element mean, the neighboring polynomials $\mathcal{P}_0$ and $\mathcal{P}_2$ requires modification,

$$\tilde{\mathcal{P}}_{j-1} = \mathcal{P}_{j-1} - \bar{\mathcal{P}}_{j-1} + \bar{\mathcal{P}}_j, \quad \tilde{\mathcal{P}}_{j+1} = \mathcal{P}_{j+1} - \bar{\mathcal{P}}_{j+1} + \bar{\mathcal{P}}_j \tag{16}$$

where $\bar{(\cdot)}$ denotes the elemental mean value of a polynomial. Then, the limited polynomial on element e_j is defined by a convex combination of these three polynomials:

$$\mathcal{P}_j^{lim} = \omega_{j-1}\tilde{\mathcal{P}}_{j-1} + \omega_j \mathcal{P}_j + \omega_{j+1}\tilde{\mathcal{P}}_{j+1} \tag{17}$$

where the normalized weights ω_j are evaluated based on the smoothness of the solution in each element. In the element with size δx, the smoothness indicator is evaluated as

$$\beta_j = \sum_{s=1}^{N} \int_{I_j} \delta x_j^{2s-1} \left(\frac{\partial^s P_j}{\partial x^s}\right)^2 dx \tag{18}$$

where N is the order of polynomial. With that, the weights can be evaluated as,

$$\omega_j = \frac{\bar{\omega}_j}{\sum_l \bar{\omega}_l}, \quad \bar{\omega}_l = \frac{\gamma_l}{(\varepsilon + \beta_l)^r}, \quad l \in [j-1, j+1]. \tag{19}$$

where ε, here set to 10^{-6}, is introduced to guarantee finiteness of $\bar{\omega}_l$, and $r = 2$ as recommended. Since the order of accuracy of each polynomial is not degraded during this linear blending, the limited polynomial is

American Institute of Aeronautics and Astronautics

expected to hold the original high-order accuracy in smooth region. Additionally, γ_{j-1}, γ_j and γ_{j+1} are set to 0.001, 0.998 and 0.001, respectively. To extend this algorithm to a equation system, it is recommended to work on the local characteristic space. To do so, we diagonalize the local flux Jacobian matrix $\mathbf{A}_j = \frac{\partial \mathbf{F}}{\partial \mathbf{U}}|_{\bar{U}_j}$, and after doing that we denote its left and right eigenvectors with $\mathbf{R}^{-1}$ and $\mathbf{R}$. The transformation to the local characteristic space V_j is done by left-multiplying $\mathbf{R}^{-1}$ to the vector of solution polynomials U_j. Once limiting is conducted on each troubled component of V_j, the limited conservative polynomial is reformed into physical space by left-multiplying $\mathbf{R}$ to V_j^{lim}.

To apply this limiting procedure to chemically reacting problem, some compatibility issue with the double flux model requires considerations. Specifically in the double flux model, each element should not be affected by the thermal property change in adjacent elements, while in this limiting process the blending of local polynomials with those in the adjacent elements will introduce the thermal property information from the neighbors. As we know, since this information is introduced from energy solution, a ghost energy solution is constructed for each neighboring element using thermal property information for element e_{j-1} and e_{j+1}. Here we take one neighbor e_{j+1} as example,

$$P_{j+1}^{ghost}(\rho E) = \frac{\gamma_{j+1} - 1}{\gamma_j - 1} \left(P_{j+1}(\rho E) - \frac{P_{j+1}^2(\rho u_i)}{2P_{j+1}(\rho)} \right) + \frac{P_{j+1}^2(\rho u_i)}{2P_{j+1}(\rho)} \tag{20}$$

where the resulting ghost energy solution most likely does not follow the form of polynomial function. If this is the case, least square fitting is applied in this neighboring element.

IV. Numerical Tests

In the following part, we would like to demonstrate the capability of our algorithm by conducting a series of numerical test. All the tests introduced here are on one-dimension.

A. Gaseous Thermal Bubble Advection

This case aims to test the treatment of the hyperbolic operator. To mimic a flame profile, the initial condition for species and temperature is given by a hyperbolic tangent profile. The length and temporal scale is defined by θ and Γ, respectively. Periodical boundary conditions are used. Initial conditions are defined as

$$
\begin{aligned}
u(x,0) &= \theta/\Gamma \\
Y_{\mathrm{H_2}}(x,0) &= 0.5 \left[1 - tanh\left(\frac{|x| - 20\theta}{2\theta} \right) \right] \\
Y_{\mathrm{O_2}}(x,0) &= 1.0 - Y_{H_2}(x,0) \\
T(x,0) &= 0.5(T_{min} + T_{max}) + 0.5(T_{min} - T_{max})tanh\left(\frac{|x| - 20\theta}{2\theta} \right) \quad \mathrm{K} \\
p(x,0) &= 1 \quad \mathrm{atm}
\end{aligned}
$$

where T_{min} and T_{max} are set to 300 K and 2000 K, respectively. For convergence analysis, the grid size varies between $\theta/0.64$ to $\theta/5.12$. Since only the hyperbolic operator is investigated, the analytical solution for this problem is simply a displacement of the initial profile. This problem inherently results in a smooth solution; therefore, no limiting is used.

Figure 2 shows the predictions obtained using polynomial P1, P2 and P3 on the coarsest grid. As the polynomial order increases, the results show significant improvements. The linear approximation with P1 introduces oscillations which diminish for P2 and P3. With the double flux method, spurious oscillations are eliminated as shown by the pressure profile in the bottom-left subplot of Fig. 2. The energy conservation errors are also shown as a function of simulation time for three different polynomials on two grid sizes. It is clear that the conservation error drops with refinement. As the simulation advances, the error based on P1 experiences slight growth, but the errors with higher polynomials shows very stable behavior. When the grid is refined, the error reduces fast. The behavior on relatively coarse grid may be explained from the viewpoint of numerical dissipation. Higher order polynomials result in less dissipation than lower orders in DG. Nevertheless, energy convervation errors are all less then 5×10^{-4} % at the end of the simulation.

Table 1 shows the results from a convergence analysis for this test case for polynomials of different order. As expected, the errors in the L_2-norm for temperature and hydrogen mass fraction both show optimal convergence rate of $P+1$.
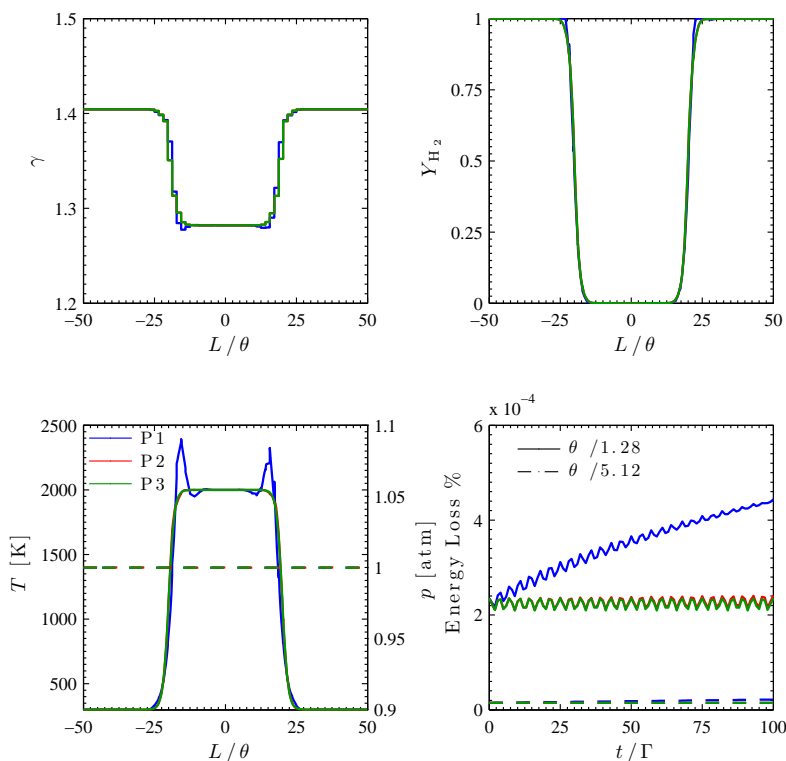

Figure 2. Simulation result of gaseous thermal bubble advection for three different polynomials; top-left, profile of heat capacity ratio; top-right, profile of hydrogen mass fraction; bottom-left, profiles of temperature and pressure; bottom-right, energy conservation error as a function of time.

	Y_{H_2}		T	
	L_2 norm error	Convergence rate	T L_2 norm error	Convergence rate
P1, $\theta/0.64$	90.45	-	1.466e-2	-
P1, $\theta/1.28$	22.74	1.99	7.989e-3	0.87
P1, $\theta/2.56$	3.548	2.68	1.926e-3	2.05
P1, $\theta/5.12$	4.576e-1	2.95	2.552e-4	2.92
P2, $\theta/0.64$	7.332	-	3.925e-3	-
P2, $\theta/1.28$	3.730e-1	4.30	1.466e-4	4.74
P2, $\theta/2.56$	1.576e-2	4.56	6.700e-6	4.45
P2, $\theta/5.12$	1.452e-3	3.44	6.471e-7	3.37
P3, $\theta/0.64$	4.397e-1	-	8.534e-5	-
P3, $\theta/1.28$	6.498e-3	6.08	3.115e-6	4.77
P3, $\theta/2.56$	2.691e-4	4.59	1.514e-7	4.36
P3, $\theta/5.12$	1.675e-5	4.01	9.452e-9	4.00

Table 1. Grid convergence study for gaseous thermal bubble advection using three polynomials of different order

American Institute of Aeronautics and Astronautics

B.   Multi-species Shock-tube Problem

This problem is constructed to test the shock-capturing capability and its compatibility with the treatment of variable thermodynamics properties. In a shock-tube, we consider two gaseous, helium and nitrogen, that are initially separated in a left and right states, having the following conditions:

$$
\begin{aligned}
T_L &= 300 \text{ K}, & T_R &= 300 \text{ K}, \\
u_L &= 0 \text{ m/s}, & u_R &= 0 \text{ m/s}, \\
p_L &= 10 \text{ atm}, & p_R &= 1 \text{ atm}, \\
Y_{\text{He,L}} &= 1, & Y_{\text{He,R}} &= 0, \\
Y_{\text{N}_2,\text{L}} &= 0, & Y_{\text{N}_2,\text{R}} &= 1,
\end{aligned}
$$

Initial discontinuity is placed at $x = 0.4$ m, and the entire computational domain is 1m. In this simulation, the CFL number is set to 0.3 and the constant M for the shock detector is set to 50. The simulation is performed up to 300μs, and two different meshes are considered.

   As for this problem, there is no analytical solution since thermal properties are now a function of species composition. However, the post-shock state could be computed according to the procedure proposed by John.[12] Quantitative comparisons between the simulation result and the exact post-shock state are listed in Table 2. As observed, the discrepancy between the DG solution and reference data is very subtle. The critical features are well resolved based on the developed scheme, which is also shown in Figure 3. No spurious oscillations are observed in the pressure profile. Also, with increasing grid resolution, the shock become better resolved. Since shock-capturing is adopted, no higher order polynomials are used in this case. The right part of Figure 3 shows the energy conservation error as a function of time for different grid sizes.The reduction in error is apparent as grid size reduces, and the energy conservation errors are less than of 2×10^{-3}. Although P1 and P2 both capture the correct physics, due to the nature of this problem, there is no extra benefits of using higher order polynomial. Obviously, the fully conservative formulation gives a wrong solution for this problem due to the introduction of numerical errors, which shows oscillating behavior for the density and under-predict the value of the post-shock pressure.

Variable	Post-Shock Data[12]	P2, 2mm	Error [%]	P1, 2mm	Error [%]
p [MPa]	0.4617	0.4609	0.17	4.609	0.17
ρ [kg/m^3]	3.03	3.05	0.66	3.05	0.66
T [K]	513.1	508.8	0.84	508.8	0.84
u [m/s]	444.7	445.5	0.18	445.2	0.11
u_{shock} [m/s]	712.0	708.2	0.53	708.7	0.46

Table 2.   Comparison of predicted post-shock results for 1D He/N$_2$ shock tube problem.

C.   Multi-species Density Wave

This example is introduced by Shu[13] to demonstrate the effectiveness of using higher-order scheme in shock involved problem. All the values in this problem are non-dimensionalized already. The initial condition is defined as

$$
\begin{aligned}
\rho_L &= 3.857143, & \rho_R &= 1 + 0.2sin(5x), \\
u_L &= 2.629369, & u_R &= 0, \\
p_L &= 10.333333, & p_R &= 1, \\
Y_{He,L} &= 1, & Y_{He,R} &= 0, \\
Y_{N_2,L} &= 0, & Y_{N_2,R} &= 1,
\end{aligned}
$$

which results in the interaction of a Mach 3 shock and a density wave. The initial discontinuity is located at $x = -4$. Since the shock and smooth regions are present in this problem, the challenge is not only to capture the shock but also to describe the solution in the smooth region accurately. The "exact" solution is obtained using 1000 cells with P2. As shown in Fig. 4, P2 and P1 solutions both predict the locations of the
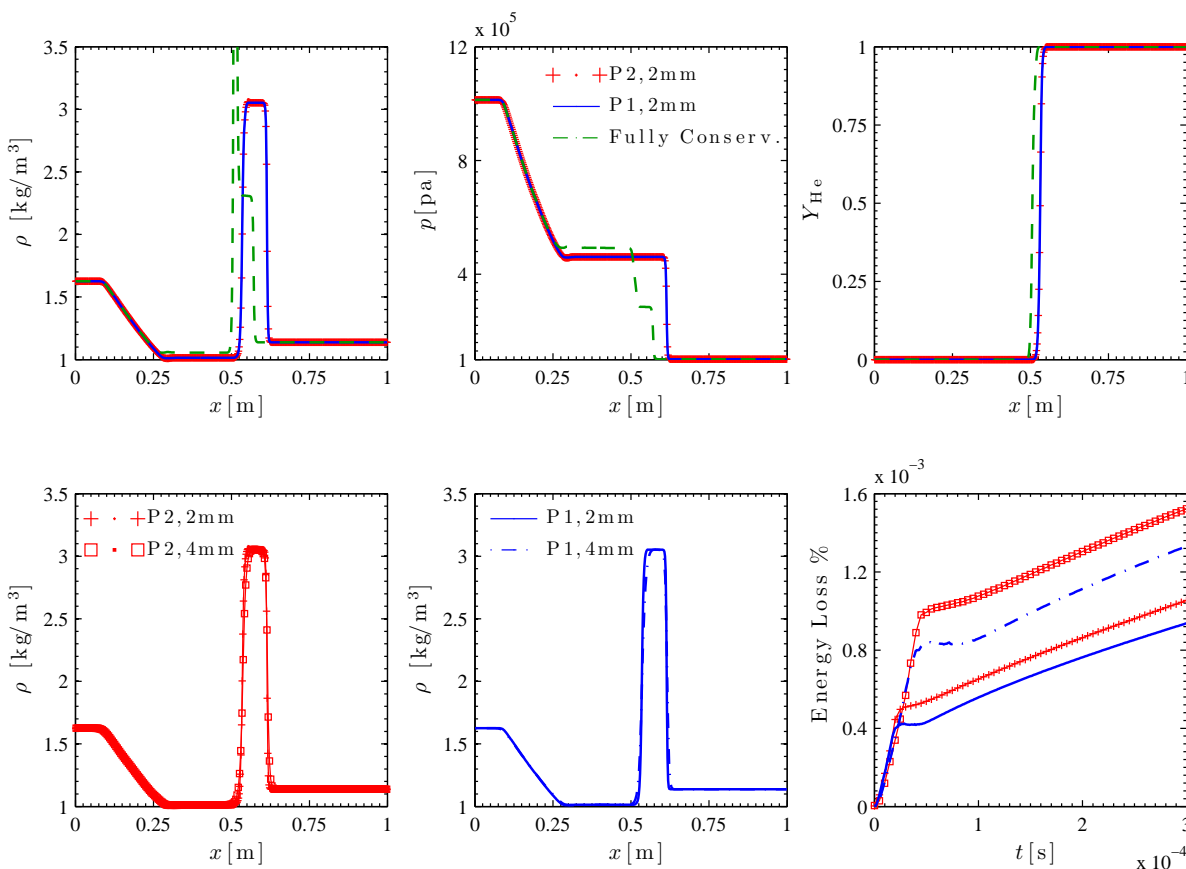
American Institute of Aeronautics and Astronautics

Figure 3. Results of multi-species shock tube test case for P1 and P2

shock and also the contact discontinuity. However, inside the density wave, P2 performs considerably better than P1 in terms of capturing the higher frequencies of the density wave. In this case, P2 also introduces less energy conservation error compared with P1.

D. Multi-species Detonation Problem With Detailed Reaction Chemistry

This case is designed to test whether the developed scheme is able to capture the supersonic combustion wave. The $H_2/O_2/Ar$ mixture with molar ratio of 2:1:7 is initially homogeneous in 1D domain, with pressure and temperature of 6670 Pa and 289 K, respectively. After ignition, the system transitions to a steady-state Chapman-Jouget detonation wave. This case has been studies by Oran et al.[14] and Deiterding[15] using reduced and detailed chemistry, respectively. In the present work, a 9-species and 34-step reaction mechanism[16] is used involving all critical radicals, such as OH, H, O, and HO_2.

To ignite the mixture, CJ condition is initially imposed as a discontinuity. To handle stiff chemistry, an ODE solver is employed, combined with a time-splitting integration scheme. Four cases are predicted on two different grids. The coarser grid is 150 μm for P2 and 100 μm for P1, while the finer set is 75 μm for P2 and 50 μm for P1. This configuration can guarantee the same degree of freedom for P1 and P2 on each grid. The CFL number is set to 0.5 for all runs. Since there is no exact solution for this case, a reference calculation from Deiterding[15] is used for comparison.

Computational results for this simulation are presented in Fig. 5. With all simultions, the Zeldovich-Neumann-Döring (ZND) structure is well captured. It can been seen that the reaction zone is resolved equally well for P1 and P2 on the finer grid set with the same number of degrees of freedom. The P2 simulation saves about 12.5 % CPU-time compared to P1. However, if we focus on the shock front only, the resolution only depends on the grid size and not the polynomial order. Further, the Von Neumann pressure and temperature is observed clearly from the ZND structure. After the detonation wave reaches a quasi-
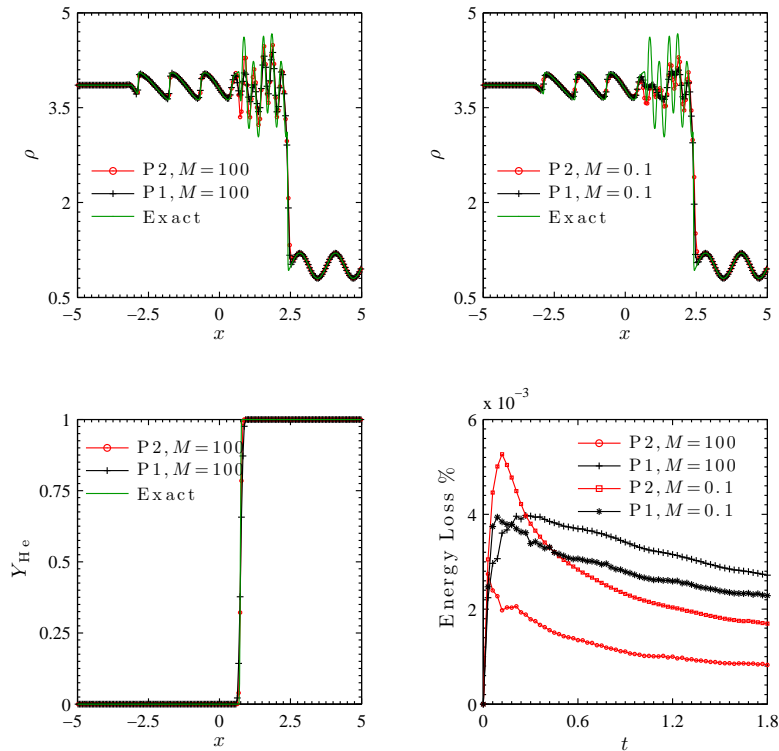
Figure 4. Results of multi-species density wave test case for P1 and P2 (M constant in WENO-limiter)

steady state, the values for the Von Neumann pressure, temperature and detonation speed are evaluated and compared with the results from a FV computation.[15] The convergence results with the finer grid set is listed in Tab. 3.

Variable	Prediction (P2, 75 μm)	Prediction (P1, 50 μm)	Reference Data[15]
p_{vn} [kPa]	183.8	183.5	177.3
T_{vn} [K]	1974.2	1965.7	1921.7
u_{det} [m/s]	1667.2	1665.7	1626.9

Table 3. Comparison between predicted and reference results[15] for $H_2/O_2/Ar$ detonation wave.

V.   Conclusions

In this work, a discontinuous Galerkin method for simulating realistic detonation and supersonic combustion systems was developed. The presented algorithm accurately treats temperature- and mixture-dependent thermodynamic properties using a double-flux formulation, stiff multi-species chemistry using a time-splitting scheme, and provides shock-capturing capabilities using a WENO-limiter. The capability and accuracy of the algorithm were assessed and demonstrated in applications to a series of time-dependent test-cases of increasing physical complexity. Simulations of a multi-species Argon-diluted Hydrogen/Oxygen system were conducted by considering detailed chemical-kinetics, and it was shown that the developed numerical method achieves optimal convergence rate, demonstrates robust shock-capturing ability and accurately represents the multi-species flame-structure in smooth regions. While it was shown that the ZND-flame structure behind the shock is well predicted and in agreement with results from FV-simulations, it was also demonstrated that high-order polynomial representations in this region can further improve the accuracy and simultaneously
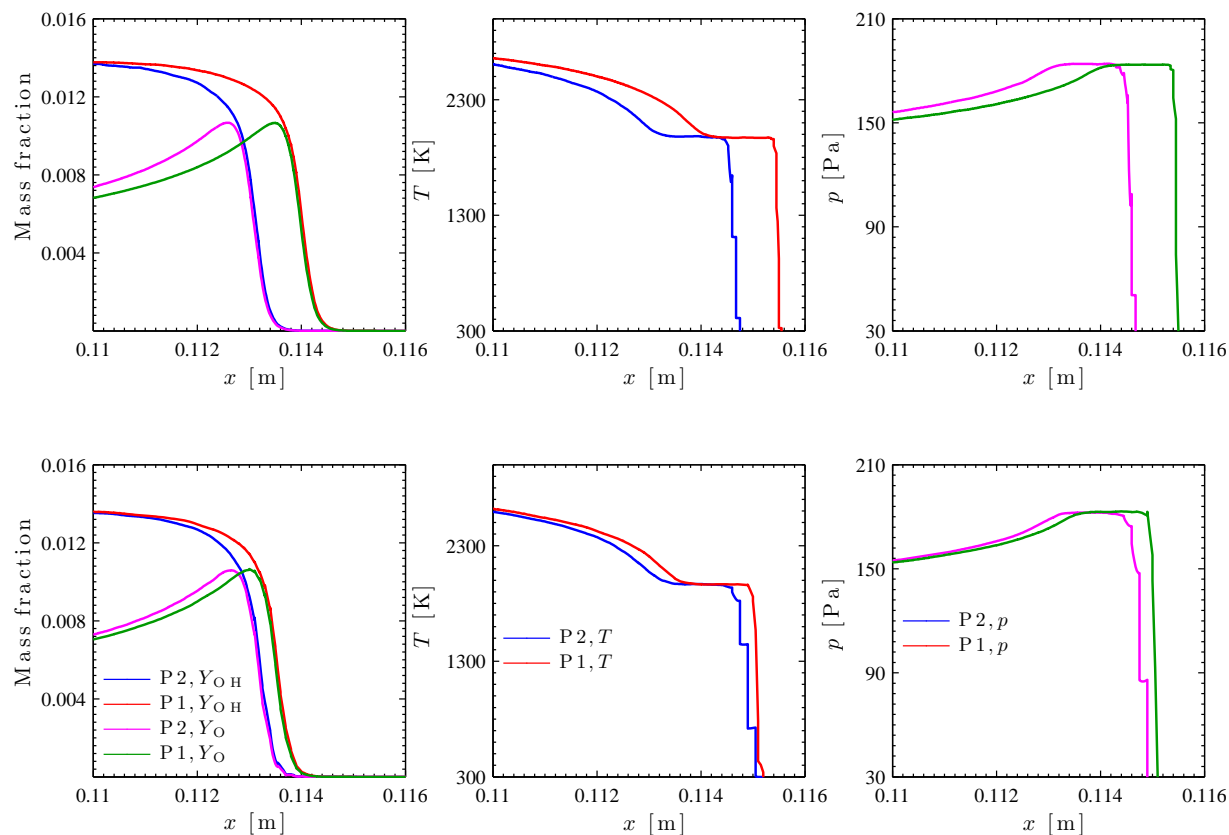
American Institute of Aeronautics and Astronautics

Figure 5. Results of multi-species detonation for P1 and P2: upper, finer grid; lower, coarser grid.

reduce the computational cost. Future work will address the extension to multi-dimensional systems and the consideration of hp-refinement strategies.

Acknowledgments

References

[1]Billet, G. and Ryan, J., "A RungeKutta discontinuous Galerkin approach to solve reactive flows: The hyperbolic operator," *Journal of Computational Physics*, Vol. 230, No. 4, 2011, pp. 1064–1083.

[2]Zhong, X. and Shu, C.-W., "A simple weighted essentially nonoscillatory limiter for RungeKutta discontinuous Galerkin methods," *Journal of Computational Physics*, Vol. 232, 2013, pp. 397–415.

[3]Kee, R. J., Rupley, F. M., Miller, J. A., Coltrin, M. E., Grcar, J. F., Meeks, E., Moffat, H. K., Lutz, A. E., Dixon-Lewis, G., Smooke, M. D., Warnatz, J., Evans, G. H., Larson, R. S., Mitchell, R. E., Petzold, L. R., Reynolds, W. C., Caracotsios, M., Stewart, W. E., and Glarborg, P., "Chemkin Collection, Release 3.5," 1999.

[4]Van Leer, B., "Towards the ultimate conservative difference scheme V. A second-order sequel to Godunov's method," *Journal of Computational Physics*, Vol. 32, No. 1, 1979, pp. 101–136.

[5]Shyue, K. M., "An efficient shock-capturing algorithm for compressible multicomponent problems," *Journal of Computational Physics*, Vol. 142, 1998, pp. 208–242.

[6]Wang, S. P., Anderson, M. H., Oakley, J. G., Corradini, M. L., and Bonazza, R., "A thermodynamically consistent and fully conservative treatment of contact discontinuities for compressible multicomponent flows," *Journal of Computational Physics*, Vol. 195, 2004, pp. 528–559.

[7]Fedkiw R., Aslam T., M. B. and Osher, S., "A non-oscillatory Eulerian approach to interface in multi material flows (the Ghost Fluid Method)," *Journal of Computational Physics*, Vol. 152, 1999, pp. 457–492.

[8]Mulder, W. Osher, S. and Sethian, J., "Computing interface motion: The compressible Rayleigh-Taylor and Kelvin-Helmholtz instabilities," *Journal of Computational Physics*, Vol. 100, 1992, pp. 209–228.

[9]Abgrall, R. and Karni, S., "Computations of Compressible Mulitfluids," *Journal of Computational Physics*, Vol. 169, 2001, pp. 594–623.

[10]Abgrall, R., "How to prevent pressure oscillations in multicomponent flow calculations: a quasi conservative approach," *Journal of Computational Physics*, Vol. 125, 1996, pp. 150–160.

[11]Cockburn, B. and Shu, C. W., "TVB Runge-Kutta local projection discontinuous Galerkin finite element method for conservation laws III: One dimensional systems," *Journal of Computational Physics*, Vol. 84, 1989, pp. 90–113.

[12]John, J., "Gas Dynamics," (second ed.)Prentice Hall, Upper Saddle River, NJ, 1984.

[13]Shu, C.-W. and Osher, S., "Efficient implementation of essentially non-oscillatory shock-capturing schemes II," *Journal of Computational Physics*, Vol. 83, 1989, pp. 32–78.

[14]Oran, E. S., Weber, J. W., Stefaniw, E. I., Lefebvre, M. H., and Anderson Jr, J. D., "A numerical study of a two-dimensional H2-O2-Ar detonation using a detailed chemical reaction model," *Combustion and Flame*, Vol. 113, No. 1-2, 1998, pp. 147163.

[15]Deiterding, R., "Parallel adaptive simulation of multi-dimensional detonation structures," Ph.D. Thesis, Branderburg University of Technology Cottbus, 2003.

[16]Westbrook, C. K., "Chemical kinetics of hydrocarbon oxidation in gaseous detonations," *Combustion and Flame*, Vol. 46, 1982, pp. 191–210.

American Institute of Aeronautics and Astronautics